Mineralogy and Geochemistry of the Kinnikinic Quartzite at the Arco Hills Silica and Gold Project in Butte County, Idaho: Results of an Ore Quality Spot Check and Implications for Potential Plasma Furnace Processing

Carter Lindeman [1,2], Traister Oglesbee [1,2], Claire McLeod [2] and Mark P.S. Krekeler [1,2,*]

[1]   Department of Mathematical and Physical Sciences, Miami University Hamilton, Hamilton, OH 45011, USA; lindemcr@miamioh.edu (C.L.); oglesbta@miamioh.edu (T.O.)

[2]   Department of Geology & Environmental Earth Science, Miami University, Oxford, OH 45056, USA; mcleodcl@miamioh.edu

[*]   Correspondence: krekelmp@miamioh.edu

Abstract: Plasma furnace processing has the potential to transform solar cell production. If informed decisions regarding silicon ore and mineral exploration can be made such that waste streams are also of high economic value, then production is ultimately more environmentally integrated. This study presents results from a spot check of the Kinnikinic Quartzite, ~4.5 km east of Arco, Butte County, Idaho (43.639091°, −113.243295°), for ore quality. The mineralogical and geochemical characteristics are explored within the context of a planned plasma furnace project at the sampled site and are compared to previous consulting reports. X-ray diffraction analysis detected only quartz, while scanning electron microscopy identified quartz grains, secondary quartz cement, trace amounts of potassium feldspar, minor iron oxides, and secondary illite. The bulk chemical characterization of 20 samples (including repeats) reports several wt. % variation in SiO_2 from 96.47 to 99.66. Other notable chemical components include Al_2O_3, K_2O, CaO, and Rb, all consistent with the presence of potassium feldspar (and illite). Gold concentrations vary from below detection (n = 12 out of 20) to a maximum concentration of 0.086 ppm. Total sum REE concentrations vary from 13 to 143 ppm. Conservatively and optimistically, assuming ideal extraction and recovery in plasma furnace operation, a resulting waste stream would have approximately 15.2 ppm (0.488 oz./metric ton) gold and 3400 ppm REE in the average waste. Gold (and REE extraction) may, however, be complicated by the presence of Fe and Cu if cyanide approaches were implemented. Gold concentrations are significantly lower than reported in previous work, warranting further characterization of this unit locally and regionally in order to characterize ore potential. This study works to demonstrate the possibility of evaluating other potential silicon ore units, such as the St. Peter Sandstone in Illinois and Missouri, for the co-production of materials in support of an emerging green economy.

Keywords: quartzite; gold; rare earths; silicon ore; plasma furnace; green economy

1. Introduction

Valuable resources including precious metals and rare earth elements are key to the green economy as it relates to energy production, waste reduction, and pollutant degradation [1–5]. Accordingly, the maximization of exploration efforts and the assessment of non-traditional sources of ores, REEs, and precious metals are increasingly being investigated [6–10]. For example, recycling mine waste for

metals and other associated resources has become much more targeted, owing to growing economic interest over the last two decades [11–15]. Ideally, however, multiple green economy resources would be extracted synchronously, i.e. during the same mining process, in order to minimize waste and support the mitigation of economic risk owing to commodity fluctuation. For example, wide price fluctuations have occurred over the past decade for both REEs [16–18] and gold [19–21]. The study presented here stems from efforts to investigate a planned plasma furnace operation using the Kinnikinic quartzite of central Idaho [22,23]. This once proposed facility would have a primary production volume of silicon metal and several potential byproduct streams, with Au and REEs being of primary interest.

The stratigraphy of the Middle Ordovician Kinnikinic quartzite in Idaho is summarized in Figure 1 [22,23] and has been described as a fine- to medium-grained, silica-cemented, supermature quartz arenite [24].
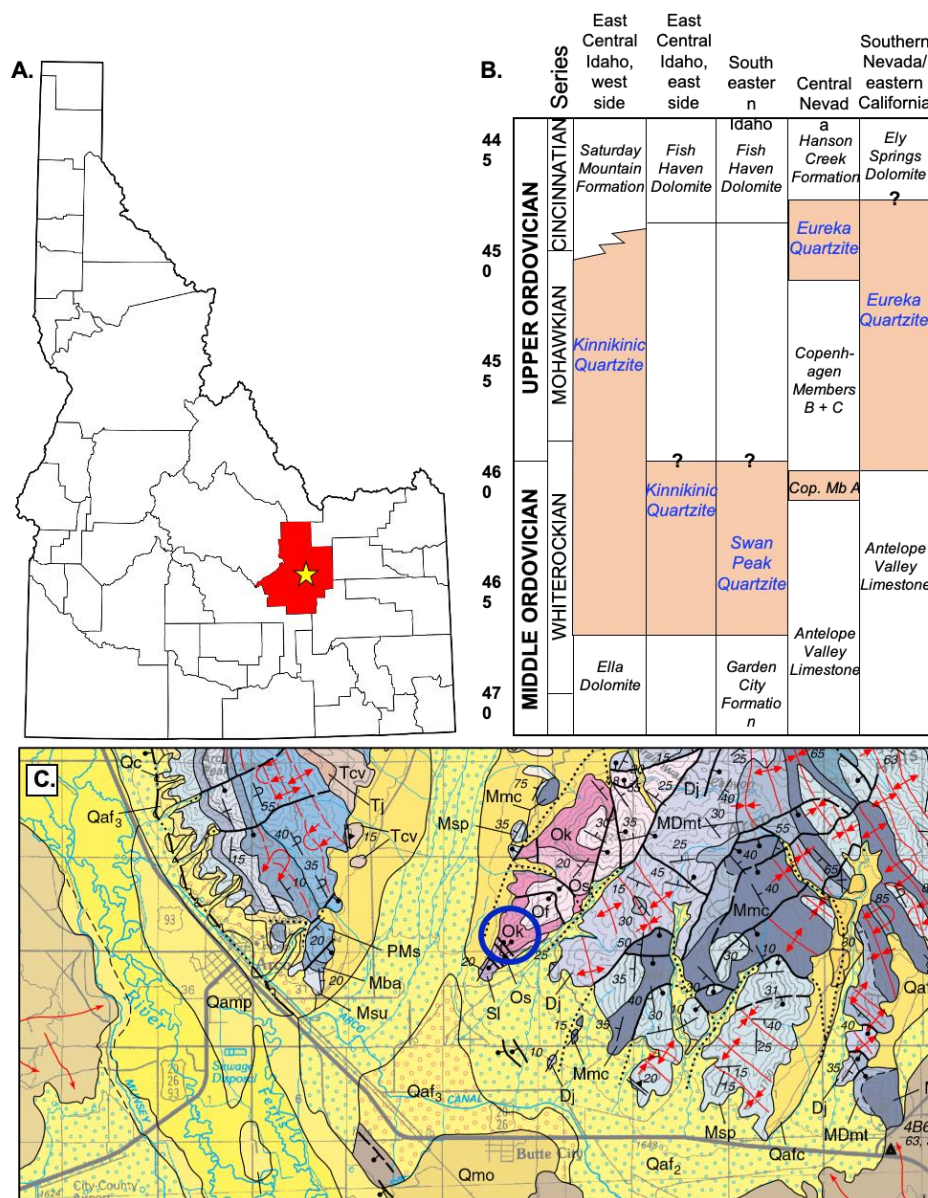
Figure 1. (**A**). State map showing the general location of the proposed Arco Hills Silica and Gold Project (AHSGP) in Butte County, Idaho [25]. (**B**). Regional Paleozoic stratigraphy for the study area [24]. (**C**). Geological map [26] of the Arco region with the sample site in the Middle Ordovician Kinnikinic Quartzite (Ok) unit identified by the blue circle (43.639091°, −113.243295°).

The depositional environment is associated with a marine, shallow-shelf, high energy setting. Within the context of the broader paleogeography, these regionally extensive arenites record a time period of siliciclastic sedimentation in an otherwise predominantly carbonate dominated regime associated with the Western Laurentian passive margin [24–27].

The formation's deposition is specifically interpreted as being associated with moderate to high-energy currents which were in a predominantly southwestward-flowing direction. The Kinnikinic quartzite is characterized by structureless beds with medium to thin parallel bedding. Within this unit parallel laminae dominate and small-scale ripples and shallow scours are rare. Skolithos tubes are uncommon and largely constitute the otherwise sparse trace-fossil assemblage. Previous studies of the Kinnikinic quartzite have focused on its provenance via study of detrital zircons. Extensive investigations of time equivalent deposits have previously been conducted [27–32]. These efforts initially supported a sole sediment source for the Kinnikinic quartzite, namely the Peace River Arch of British Columbia, identified by a prominent 1.8–2.0 Ga detrital zircon age peak. Subsequent work in East-Central Idaho identified significant age peaks in the detrital zircon record at 0.9–1.3 Ga, 1.9–2.0 Ga, in addition to peaks 2.0–2.2 Ga, and 2.4–2.9 Ga from >1400 detrital zircon analyses [24]. The identification of multiple age populations precludes the single source model previously proposed and instead supports sediment derivation from multiple sources, e.g. the Trans-Hudson Arch, neighboring Paleoproterozoic-Archean domains, and potentially even the Mesoproterozoic Belt Supergroup [24]. A more recent study assessing the entire Paleozoic and early Mesozoic passive margin stratigraphy reported a dominant age peak of c. 1.8 to 1.9 Ga, with smaller age peaks between 2.0 and 2.1 Ga and between 2.6 and 2.8 Ga [33].

While extensive geochronological constraints on the origin of the Kinnikinic quartzite (and time equivalents) exist, comprehensive mineralogical and geochemical investigations of this formation are lacking in the peer-review literature. The work presented here focuses on a suite of Kinnikinic Quartzite samples from the Arco Hills Silica and Gold Project (AHSGP) in Butte County, Idaho, within the context of validating a spot check of ore quality for a proposed plasma furnace facility. The AHSGP was a 2200-acre site and was being developed by the Arco Hills Silica Company. Previous investigations by Parkinson Geologic Services in 2009 indicated that the property contained 460 million ounces of gold and 20 billion tons of silica. From 2009 pricing, the potential gold resource was valued at $276 billion US and the accompanying silica resource was valued at $500 billion US.

From April 1998, the summary report on 13 buckets of crushed silica ore by Systems Integrated Corporation/M & W Milling and Refining, silica ore is stated to contain 0.031 oz./ton Au and trace Ag. From the June 2002 summary report of Norris Labs/M & W Milling and Refining, silica ore is stated as containing 0.012 oz./ton Au and 0.22 oz./ton Ag based on fire assay. These data also appear to be from a single sample. From the July 2002 summary report of Norris Labs/M & W Milling and Refining, selected dark materials from the silica ore, presumably Fe-oxide rich material, is stated as containing 0.398 oz./ton Au and 3.89 oz./ton Ag based on fire assay. These data also appear to be from a single sample. From three separate reports from Acme Analytical Laboratories, on 19 samples total, the silica content was determined as 97.32 to 98.48 wt. % (July 2006), 98.37 to 98.66 wt. % (July 2002) and 98.54 to 99.48 wt. % (July 2001). All of these summary reports are provided in the Supplementary Materials.

This prior work established an in-place gross value estimate of the proposed site at $776 billion, as determined by Arco Hills Silica Company, based on information provided by Parkinson Geologic Services, who reviewed the above geochemical data. Calculations were checked by Darren Kenny, CPA, using data provided by Parkinson Geologic Services and Arco Hills Silica Company (see Supplementary Materials). The Arco Hills Silica Company continued to seek development and investment of the proposed site in Butte County, Idaho. One investor group, led by Mr. Franco Palma, gained interest in developing the Butte County, Idaho site, for plasma furnace technology, in order to produce high quality Si metal for US domestic solar panel production. The aim was to use the gold byproduct generated by the waste stream to mitigate and offset operational and production costs. As part of an initial validation, Mr. Palma collected 10 large spot check samples from

the Kinnikinic quartzite associated with the planned development site in the Spring of 2014. Those samples were supplied for mineralogical and geochemical analysis and form the basis of this study. Analyses were carried out in order to evaluate previously reported silica and gold contents, as well as assess the possibilities for further resource exploration of this region.

2. Methods

2.1. Samples and Preparation

Sample material was provided by Mr. Franco Palma from a single site indicated to him to be representative of the lithology on the planned development site (personal communication). Quartzite samples were labeled 1–10 and small sub-samples were obtained for analysis via scanning electron microscopy (SEM). Duplicates (A and B) were prepared from each sample, and both were used for bulk geochemical analysis and powder X-ray diffraction (XRD) characterization. A Spex Certiprep 8000M Mixer/Mill with a tungsten-carbide grinding vial was used to powder each sample for ten minutes. Alumina and silica mills were avoided, as these were critical analytes.

2.2. Analytical Methods

Concentrations of major elements including silicon (Si) were measured on an Agilent 720ES axial-viewing inductively coupled plasma optical emission spectrometer (ICP-OES) instrument in the Department of Geology and Environmental Earth Science at Miami University [12,13]. The Si 288.1 nm is the largest Si peak on this instrument, being twice the intensity of all other Si peaks and was the wavelength used. A Rh 233.4 nm wavelength was used as the internal standard. Plasma conditions were 1.2 kW Rf power, 16.5 L/min argon plasma flow, 1.5 L/min auxiliary flow, and 0.7 L/min nebulizer flow rates. Samples were introduced to the axial torch using a SeaSpray pneumatic nebulizer and cyclonic spray chamber. Signals were integrated over six 10-second intervals.

Minor and trace element concentrations were determined on a Varian ICP-MS instrument housed in Miami University's Chemistry and Biochemistry department [12,13]. Approximately ~100 mg of sample material was weighed out into 30 mL Savillex teflon beakers, to which 2 mL of twice distilled 70% HNO_3 was added. These were tightly capped and placed on a fume hood hot plate at 120 °C for one week. The entire contents of each were then transferred into 125 mL polypropylene bottles and diluted to 125 mL, using distilled water made from a sub-boiling quartz still. Bottles and caps were pre-cleaned by rinsing in 1:1 HNO_3 acid, followed by a rinse with 18.2 megohm deionized water, and then dried in an oven at 60 °C. External calibration standards were made from 10 µg/mL solution standards purchased from Inorganic Ventures, which were diluted to 500, 50, and 5 ng/mL using 1% nitric acid. A 100 ppb solution of Ge, In, Re, and Bi was used for internal standardization. Five replicates of twenty readings each were averaged for each analytical solution.

Powder X-ray diffraction (XRD) data was collected in house in the Department of Geology and Environmental Earth Science at Miami University, using a Scintag X-1 powder diffractometer equipped with a Peltier detector, using Cu Kα2 (0.15418 nm) radiation operating at 40 kV and 35 mA. Samples were scanned from 5° to 65° 2θ at 0.02 degrees steps, using a count time of 1 s per step. The detection limit for most minerals using powder diffraction is a few weight percent.

For scanning electron microscopy (SEM) work, images and analyses were acquired using a Zeiss Supra 35 VP field emission scanning electron microscope (FESEM), at the Center for Advanced Microscopy and Imaging (CAMI), Miami University [34]. Carbon adhesive tabs were used to mount sample material on aluminum stubs. Characterization was completed using a variable pressure Zeiss Supra 35VP FEG, with nitrogen (N_2) as the compensating gas. The instrument is equipped with a backscatter detector (BSD) and an energy dispersive spectrometry (EDS) detector (EDAX2000).

3. Results

3.1. Mineralogical Results

Powder XRD patterns confirm the dominance of quartz throughout the sampled suite (Figure 2). Quartz was identified using PDF card # 00-046-1045, using the major reflections and d-values of $d_{(101)}$ = 3.3435 Å, $d_{(100)}$ = 4.2550 Å, and $d_{(112)}$ = 1.8120 Å. Only one sample, 1B, exhibited a trace peak for potassium feldspar, at approximately 3.24 Å, consistent with microcline and other feldspars [35]. Patterns show very little variation, indicating, from the perspective of bulk mineralogy, that the Kinnikinic quartzite is homogenous.
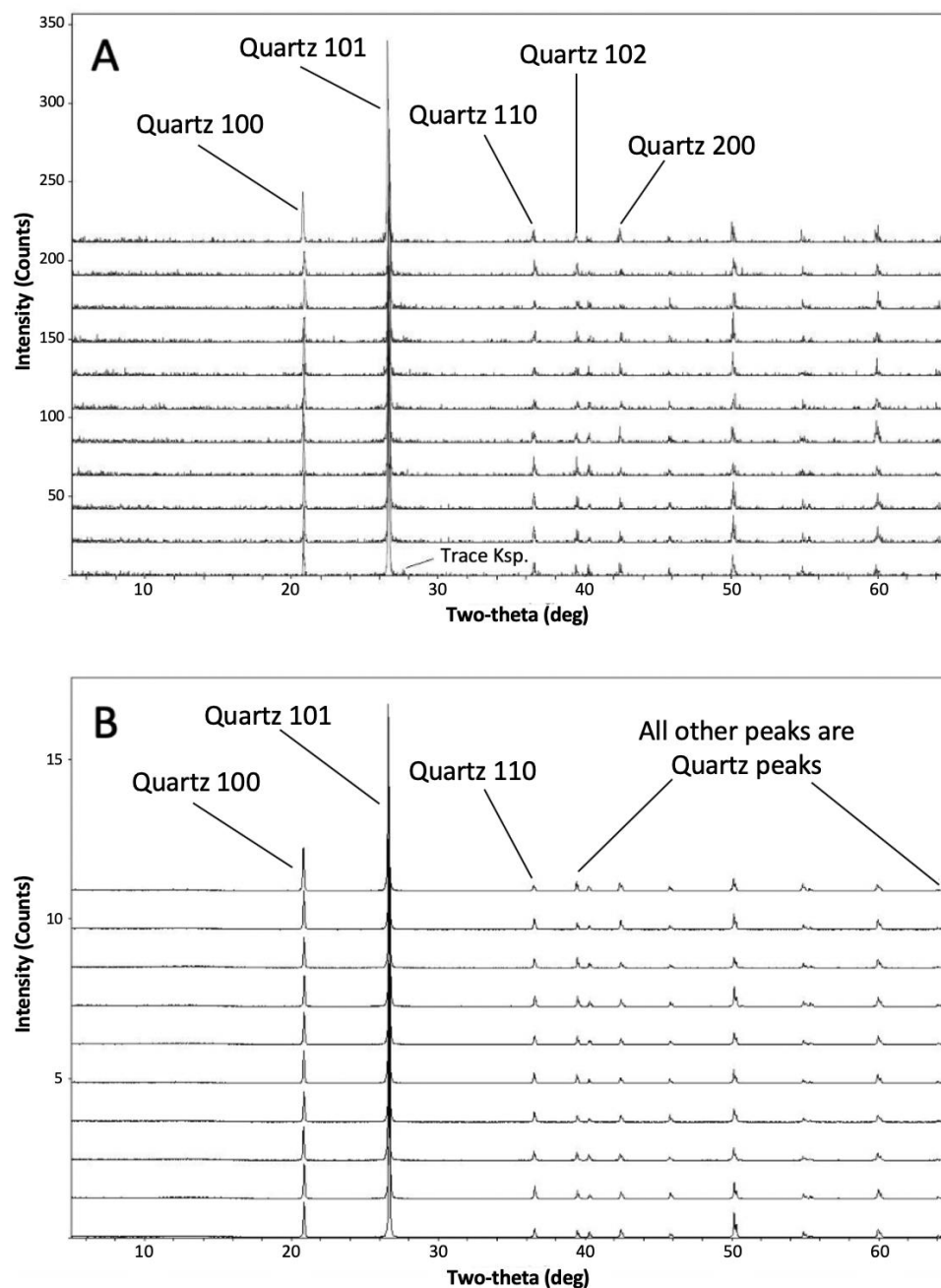
Figure 2. Powder X-ray diffraction patterns of samples 1–10B, showing only diffraction peaks for quartz. Major lines are labelled. Sample 1B, exhibited a trace peak for potassium feldspar, at approximately

3.24, consistent with microcline and other feldspars [35]. Minor K-feldspar peaks are present near detection level in some patterns.

The quartzite samples collectively consist of moderate to well-rounded detrital primary quartz grains that are held together by secondary quartz cement, as established by SEM characterization (Figures 3 and 4). This explains the high purity of the quartzite samples with respect to silica content. Several impurities do occur and include potassium feldspar, illite, and iron oxides (as documented in Figure 3). Comparatively, potassium feldspar, which is rare in the samples (Figure 3B), was investigated by SEM and illite is shown to occur as a late stage pore filling mineral after quartz cement (Figures 3C and 4C). From SEM-EDS (energy dispersive X-ray spectroscopy), illite chemical composition is dominated by potassium, aluminum, silica, and minor magnesium. Iron oxides (Figure 3D) appear to be formed at the same time as, or after, formation of the silica cement.
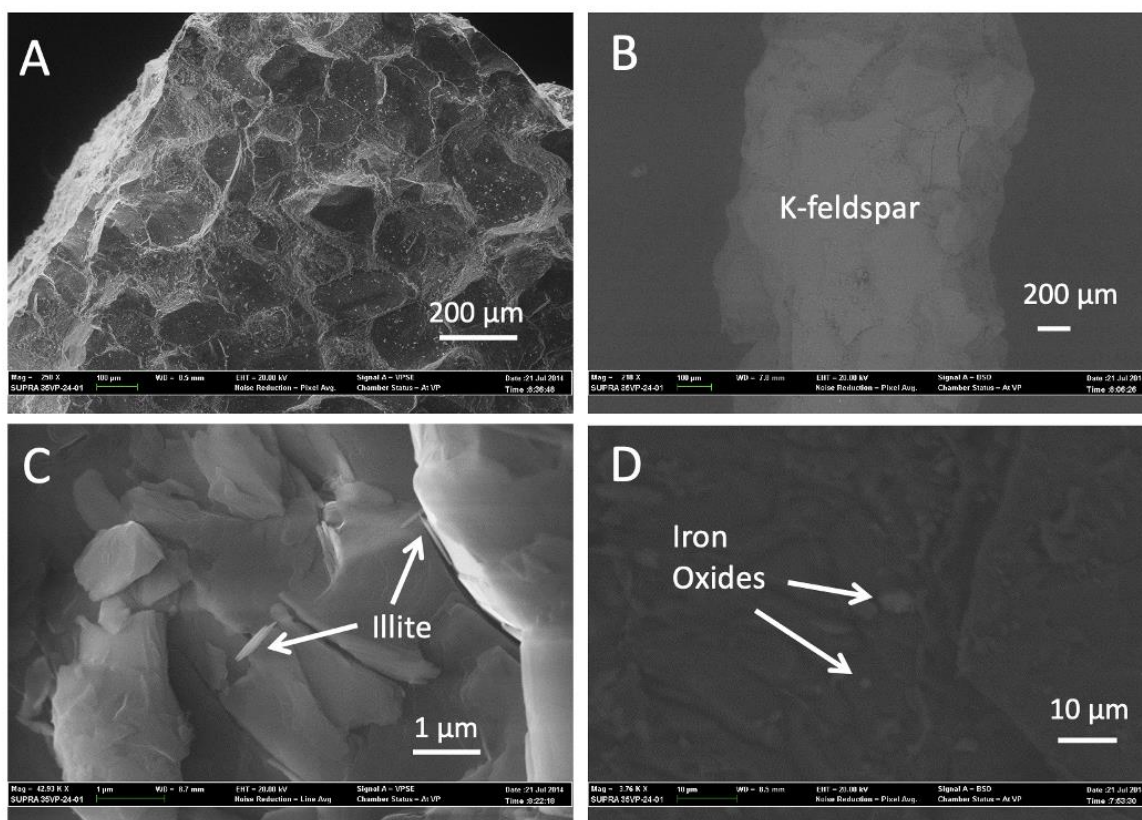
Figure 3. SEM images showing common textures and impurities are observed. (**A**) Low magnification image showing quartz grains and quartz cement as the pervasive texture. Grains are well- to sub-rounded and are approximately 100 to 300 μm in diameter. Quartz comprises more than 95% of the cement and there is no visible porosity at this scale. (**B**) K-feldspar grains are uncommon and are sub angular with fractures. When observed, they are commonly 1 mm in maximum dimension. (**C**) SEM image of cement with abundant euhedral to subhedral illite particles < 1 illite μm in diameter. This texture is predominant in samples. (**D**) Equant subhedral Fe-oxides 2 to 6 μm in diameter embedded in quartz cement.

Approximately 10% of the observed iron oxide grains contain trace amounts of titanium, consistent with the phase magnetite. Areas of the studied samples that contained iron oxides generally appeared to have lesser amounts of, or no, illite associated with them. No phases of environmental concern (such as lead sulfides, arsenic-, uranium-, mercury-bearing minerals) were observed. No gold or silver was observed.
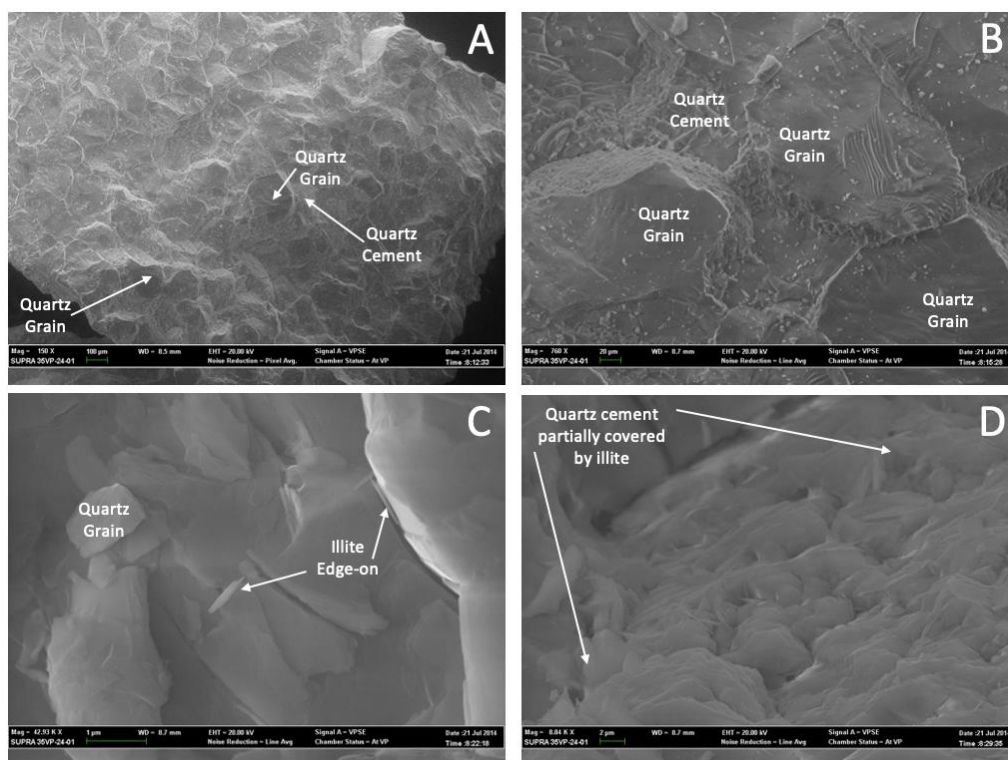
Figure 4. SEM images showing common textures and impurities observed. (**A**) A low magnification image showing quartz grains in quartz cement. Grains vary from approximately 100 to 300 μm in diameter. (**B**) A higher magnification image showing no visible macro porosity between cement and grains. (**C**) A broken surface showing small crystallites of illite on edge on a quartzite cement surface. Illite crystallites are approximately 1 μm in diameter. (**D**) A quartz cement with subhedral crystals partially covered (30%) by illite crystallites that are approximately 2 μm in diameter.

3.2. Bulk Geochemical Results

Bulk major oxide and trace element concentrations for the samples studied, including their repeats, are reported in Table 1.

The concentrations of silica, expressed here as weight percent SiO_2, varied from 96.47 wt. % to 99.66 wt. %, with an average of 99.10 wt. % and an associated standard deviation of 1.36 (n = 20, reported at 2σ). Compared to the previous Acme Analytical Laboratory reports from 2001, 2002, and 2006, these values are broadly consistent, where values, across all three reports, ranged from 97.32 wt. % to 99.48 wt. % SiO_2. Other major oxide concentrations from the samples which form the basis of this study are presented in Figure 5.

The majority of samples contain <1 wt. % of the remaining oxides, with Al_2O_3 (0.17–0.68, average: 0.38, 2σ at 0.25) and K_2O (0.028–0.188, average: 0.087, 2σ at 0.090) being the most abundant of these. This is attributed to the presence of alkali feldspar (Figure 3B). All other major oxides are present at <0.14 wt. % respectively. From Figure 5, it is shown that sample 4 contains higher total abundances of the other major oxides and correspondingly, some of the lowest wt. % SiO_2 values at 98.68 and 98.84 for replicates A and B respectively. These two replicates exhibit the highest K_2O values at 0.19 wt. % and the highest Al_2O_3 values at 0.64–0.68 wt. %. Collectively, these observations are consistent with a slightly higher abundance potassium feldspar. This is also implied by complementary trace element data. Figure 6A,B summarize the relationship between wt. % Al_2O_3 vs Rb (ppm) and wt. % K_2O vs. Rb (ppm), both of which are strongly positive (r^2 of 0.84 to 0.93).

Table 1. Bulk rock geochemical data for sampled Kinnikinic Quartzite.

(A)

Sample	SiO$_2$	CaO	Fe$_2$O$_3$	K$_2$O	MgO	MnO	Na$_2$O	P$_2$O$_5$	Al$_2$O$_3$	TiO$_2$	Total
1A	96.47	0.058	0.043	0.09	0.05	0.001	0.006	0.012	0.44	0.013	97.18
2A	99.43	0.055	0.109	0.03	0.03	<0.001	0.003	0.014	0.23	0.008	99.91
3A	99.44	0.063	0.067	0.04	0.04	b.d.	0.003	0.015	0.23	0.008	99.90
4A	98.68	0.072	0.021	0.19	0.07	b.d.	0.004	0.023	0.64	0.027	99.72
5A	99.16	0.077	0.017	0.12	0.05	b.d.	0.004	0.013	0.39	0.009	99.84
6A	99.18	0.110	0.028	0.10	0.05	b.d.	0.003	0.015	0.46	0.009	99.96
7A	99.14	0.135	0.001	0.10	0.06	b.d.	0.005	0.015	0.42	0.007	99.88
8A	99.35	0.006	0.031	0.06	0.01	<0.001	0.002	0.002	0.37	0.015	99.86
9A	99.40	0.005	0.032	0.05	0.02	<0.001	0.003	0.002	0.32	0.011	99.85
10A	99.02	0.025	0.043	0.10	0.03	<0.001	0.006	0.000	0.36	0.013	99.60
1B	98.95	0.015	0.054	0.09	0.03	0.002	0.003	0.001	0.46	0.014	99.61
2B	99.64	0.009	0.038	0.03	0.01	0.001	0.006	0.002	0.17	0.009	99.92
3B	99.66	0.007	0.017	0.03	0.01	0.001	0.002	0.001	0.25	0.009	99.99
4B	98.84	0.003	0.025	0.19	0.04	<0.001	0.003	0.005	0.68	0.033	99.82
5B	99.15	0.002	0.053	0.11	0.03	<0.001	0.002	b.d.	0.43	0.012	99.80
6B	99.26	0.020	0.026	0.09	0.02	<0.001	0.003	b.d.	0.39	0.012	99.83
7B	99.38	0.003	0.032	0.10	0.02	<0.001	0.008	b.d.	0.35	0.010	99.91
8B	99.57	0.017	0.016	0.07	0.02	<0.001	0.002	0.002	0.28	0.015	99.99
9B	99.44	0.010	0.042	0.05	0.01	<0.001	0.003	b.d.	0.28	0.011	99.86
10B	99.00	0.007	0.110	0.09	0.02	<0.001	0.002	b.d.	0.38	0.012	99.62
Max	99.66	0.135	0.110	0.19	0.07	0.002	0.008	0.023	0.68	0.033	99.99
Min.	96.47	0.002	0.001	0.03	0.01	b.d.	0.002	b.d	0.17	0.007	97.18
Avg.	99.11	0.035	0.040	0.09	0.03	0.001	0.004	0.008	0.38	0.013	99.70
St. Dv.	0.67	0.039	0.028	0.04	0.02	0.000	0.002	0.007	0.13	0.006	0.60

(B)

Sample	Sc	V	Cr	Ni	Cu	Zn	Rb	Sr	Y	Zr	Nb	Mo	Sb	Ba	La	Ce
1A	0.83	2.11	8.13	2.79	0.53	b.d.	1.56	1.53	0.94	20.32	1.44	0.08	b.d.	8.06	2.69	4.74
2A	0.50	3.00	10.01	3.51	0.22	b.d.	0.62	1.48	1.02	21.36	1.11	0.04	0.04	8.21	4.26	7.78
3A	1.02	2.66	8.62	4.04	0.59	b.d.	0.59	1.85	0.80	19.05	1.00	0.08	0.02	7.76	6.02	12.94
4A	1.24	1.36	19.42	2.70	0.62	b.d.	2.41	1.57	2.28	32.76	0.91	0.16	b.d.	7.39	14.54	50.21
5A	0.86	1.71	8.87	2.94	0.52	10.90	1.58	1.36	1.17	17.48	0.59	0.03	0.01	5.06	3.62	4.67
6A	0.87	1.95	9.90	4.15	1.45	22.31	1.48	1.27	0.94	18.97	0.63	0.04	0.07	8.06	2.94	4.98
7A	0.82	1.78	9.95	3.74	0.25	16.12	1.24	1.25	0.64	17.51	0.59	0.03	b.d.	4.79	3.47	5.85
8A	0.91	1.72	11.07	5.03	0.51	b.d.	0.89	1.31	1.00	22.03	0.51	0.05	0.02	5.60	4.18	8.89
9A	0.53	1.79	10.31	5.08	1.16	55.93	0.81	1.27	0.88	13.42	0.37	0.18	b.d.	5.14	3.34	5.96
10A	0.75	1.90	12.47	6.63	4.80	58.23	1.59	1.69	1.13	12.56	0.62	0.06	b.d.	9.50	3.47	6.02
1B	1.07	2.48	14.07	5.97	0.37	2.10	1.62	1.43	1.44	14.95	0.64	0.07	b.d.	7.70	2.82	5.02
2B	0.72	1.71	10.35	5.42	0.23	29.58	0.67	1.58	0.68	22.13	0.55	b.d.	b.d.	7.27	4.75	8.63
3B	1.17	1.86	11.04	6.26	0.25	36.25	0.42	1.77	0.75	18.79	0.73	b.d.	b.d.	6.94	6.05	13.07
4B	1.33	1.91	22.74	4.31	0.49	27.28	2.69	1.62	2.25	40.81	0.94	b.d.	b.d.	7.78	11.36	38.08
5B	0.94	1.97	13.90	5.81	0.32	17.84	1.65	1.35	1.13	16.88	0.54	0.03	b.d.	5.09	3.93	5.04
6B	1.18	4.11	11.28	5.85	1.87	136.49	1.49	1.33	0.87	19.81	0.53	0.21	0.01	7.90	3.27	4.71

Table 1. *Cont.*

(B)

| Sample	Sc	V	Cr	Ni	Cu	Zn	Rb	Sr	Y	Zr	Nb	Mo	Sb	Ba	La	Ce
7B	1.18	3.68	12.77	6.04	0.51	12.83	1.78	1.30	0.85	15.33	0.49	0.44	b.d.	4.65	4.34	6.62
8B	0.56	1.45	15.69	7.32	1.28	7.80	1.10	1.42	0.99	18.52	0.42	0.02	b.d.	5.57	4.28	9.22
9B	0.66	1.86	11.86	10.06	0.77	95.80	0.99	1.26	0.82	16.03	0.34	0.20	b.d.	4.82	4.05	7.30
10B	0.80	3.21	15.96	7.74	0.89	139.52	1.39	1.29	0.86	17.30	0.40	0.25	b.d.	7.88	3.42	5.79
Max	1.33	4.11	22.74	10.06	4.80	139.52	2.69	1.85	2.28	40.81	1.44	0.44	0.07	9.50	14.54	50.21
Min.	0.50	1.36	8.13	2.70	0.22	b.d.	0.42	1.25	0.64	12.56	0.34	b.d.	b.d.	4.65	2.69	4.67
Avg.	0.90	2.21	12.42	5.27	0.88	44.60	1.33	1.45	1.07	19.80	0.67	0.11	0.03	6.76	4.84	10.78
St. Dv.	0.24	0.75	3.71	1.85	1.03	44.97	0.59	0.18	0.45	6.50	0.28	0.11	0.02	1.49	2.96	11.84
Sample	**Sc**	**V**	**Cr**	**Ni**	**Cu**	**Zn**	**Rb**	**Sr**	**Y**	**Zr**	**Nb**	**Mo**	**Sb**	**Ba**	**La**	**Ce**
1A	0.52	1.99	0.35	0.05	0.19	0.17	0.04	0.09	0.02	0.12	0.02	0.45	0.07	0.26	0.22	0.18
2A	0.90	3.36	0.46	0.06	0.23	0.15	0.03	0.09	0.02	0.13	0.02	0.51	0.09	0.04	b.d.	0.13
3A	1.73	7.36	1.09	0.14	0.41	0.17	0.03	0.08	0.01	0.09	0.01	0.43	0.05	0.07	b.d.	0.13
4A	8.34	39.17	9.87	1.19	3.72	0.77	0.10	0.27	0.04	0.27	0.04	0.82	0.00	0.23	1.16	0.32
5A	0.71	2.61	0.47	0.07	0.30	0.22	0.04	0.09	0.02	0.12	0.02	0.38	0.02	0.13	0.00	0.14
6A	0.54	1.87	0.30	0.04	0.18	0.17	0.04	0.09	0.02	0.11	0.01	0.42	0.02	0.14	0.14	0.20
7A	0.63	2.19	0.37	0.05	0.20	0.12	0.02	0.06	0.01	0.08	0.01	0.38	b.d.	b.d.	b.d.	0.15
8A	1.10	4.21	0.77	0.11	0.36	0.20	0.04	0.10	0.02	0.13	0.02	0.53	0.02	0.09	0.14	0.20
9A	0.71	2.65	0.46	0.06	0.22	0.14	0.03	0.08	0.02	0.10	0.01	0.30	b.d.	0.03	b.d.	0.14
10A	0.72	2.68	0.47	0.06	0.25	0.23	0.04	0.10	0.02	0.12	0.02	0.29	b.d.	0.50	0.02	0.15
1B	0.56	2.04	0.37	0.05	0.21	0.22	0.05	0.13	0.03	0.18	0.03	0.34	0.02	0.25	0.05	0.18
2B	1.00	3.67	0.50	0.07	0.25	0.11	0.02	0.06	0.01	0.07	0.01	0.50	b.d.	0.04	b.d.	0.12
3B	1.75	7.69	1.13	0.14	0.42	0.14	0.03	0.07	0.01	0.08	0.01	0.42	b.d.	b.d.	b.d.	0.11
4B	6.29	29.61	7.53	0.90	2.72	0.64	0.09	0.25	0.04	0.28	0.04	0.97	b.d.	0.29	0.87	0.31
5B	0.74	2.76	0.52	0.07	0.29	0.20	0.04	0.09	0.02	0.11	0.02	0.36	b.d.	0.18	b.d.	0.13
6B	0.53	1.91	0.31	0.04	0.17	0.15	0.03	0.08	0.02	0.10	0.01	0.44	b.d.	b.d.	b.d.	0.14
7B	0.69	2.37	0.39	0.06	0.23	0.14	0.03	0.07	0.02	0.10	0.01	0.33	b.d.	b.d.	b.d.	0.14
8B	1.15	4.47	0.83	0.11	0.38	0.20	0.04	0.09	0.02	0.12	0.02	0.43	b.d.	0.11	0.12	0.18
9B	0.84	3.14	0.52	0.06	0.25	0.15	0.03	0.08	0.01	0.09	0.01	0.38	b.d.	b.d.	0.12	0.14
10B	0.67	2.55	0.43	0.06	0.22	0.16	0.03	0.08	0.02	0.11	0.01	0.39	b.d.	0.01	0.09	0.18
Max	8.34	39.17	9.87	1.19	3.72	0.77	0.10	0.27	0.04	0.28	0.04	0.97	0.09	0.50	1.16	0.32
Min	0.52	1.87	0.30	0.04	0.17	0.11	0.02	0.06	0.01	0.07	0.01	0.29	b.d.	b.d.	b.d.	0.11
Ave.	1.51	6.42	1.36	0.17	0.56	0.22	0.04	0.10	0.02	0.13	0.02	0.45	0.04	0.16	0.27	0.17
St. Dv.	2.04	9.83	2.55	0.30	0.93	0.17	0.02	0.06	0.01	0.06	0.01	0.17	0.03	0.13	0.38	0.06

First, these overall trends, where all samples are considered, are consistent with the variable presence of potassium feldspar (where Rb is incorporated into its crystal structure). Second, the highest concentrations of Rb (ppm) are found in samples 4A and 4B, at 2.41 and 2.49. Furthermore, shown in Figure 6 is the strong correlation between Zr (ppm) and Hf (ppm) at $r^2 = 0.99$. This is interpreted to reflect the presence of volumetrically trace amounts of accessory zircon which incorporates Hf into its crystal structure (D_{Hf} in zircon >900 [36]). Samples 4A and 4B are consistently higher, with Zr (ppm) at 32–41 and Hf at 0.82–0.97.
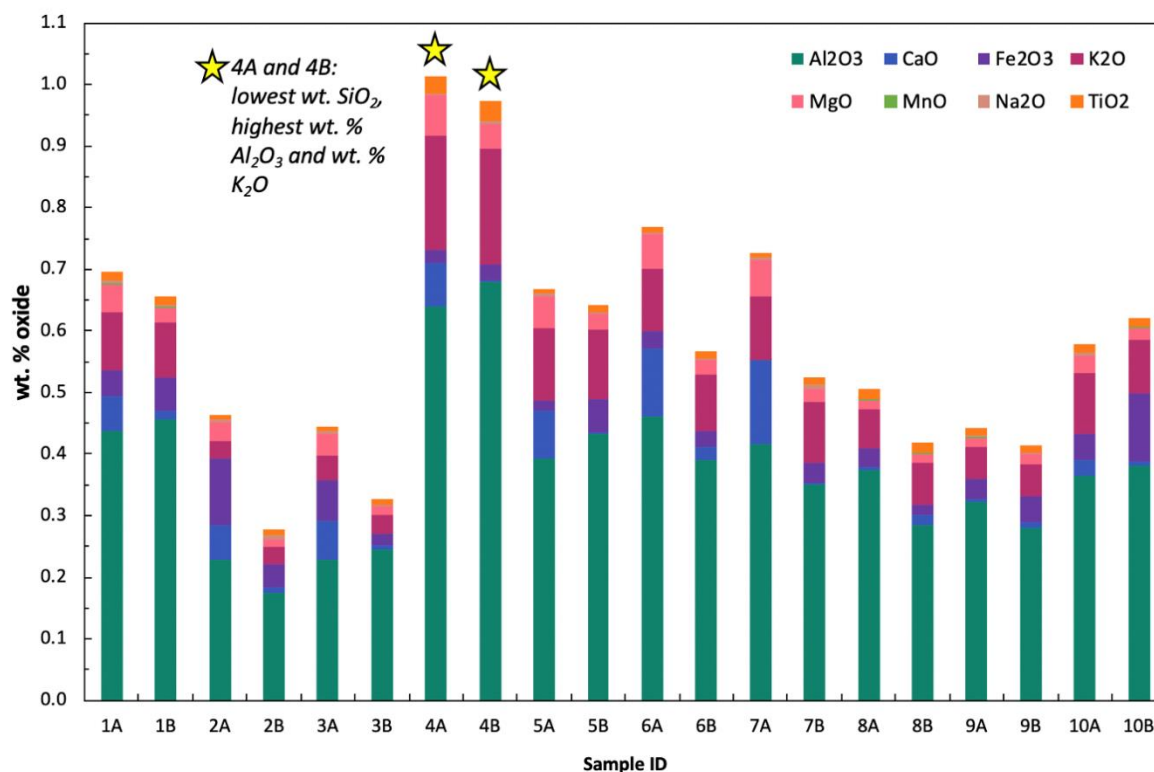
Figure 5. Major element oxide content of sampled Kinnikinic Quartz (wt. % SiO_2 not shown, see text for discussion). K_2O and Al_2O_3 contents characterize the majority of a sample's bulk major oxide composition shown here, consistent with the presence of potassium feldspar. Fe_2O_3 and MgO contents are inferred to be associated with Fe-oxides, as identified via SEM-EDS.

In Figure 6D, gold concentrations are shown vs. wt. % Fe_2O_3 (for samples in which gold was detected). Of the 20 samples analyzed, gold was detected in eight. It is also noted here that of those eight samples, seven of them are associated with the "A" split, hence, only one sample repeatedly returned detectable gold (Samples 1A and 1B). A maximum concentration of 0.086 ppm (0.003 oz./ton) is reported in sample 2A. When above detection, there appears to be weak correlation with Fe content as summarized in Figure 4D, indicating a potential association. However, this correlation is not statistically very strong ($r^2 = 0.669$, p = 0.076). No gold was detected using SEM-EDS in any sample material and no gold was found to be associated with the Fe-oxides. If present in Fe-oxides (see later), the heterogenous distribution of Fe-oxides throughout the quartzite samples could potentially account for the, albeit it statistically weak, trend in Figure 6D.

In Figure 7A–D, the compositions of the sampled quartzite are shown normalized to Earth's crustal geochemical reservoirs: bulk, upper, middle, and lower continental crust [37]. As shown, the majority of sampled quartzites are relatively depleted in all of the trace elements shown when compared Earth's crustal reservoirs by 1–3 orders of magnitude, with particularly notable depletions in Th and Sr. The overall normalized trace element patterns of the majority of samples (n = 18) are similar, with no distinguishing features which could otherwise be used to discern samples from one another. The only exception to these observations are samples 4A and 4B, which overall exhibit similar patterns to the rest of the sample suite, with several notable differences: relative enrichments in Th, La, Ce, Nd, Sm, and Eu. Only Nd and Sm are consistently >1 when normalized to crustal reservoirs, but never >4.
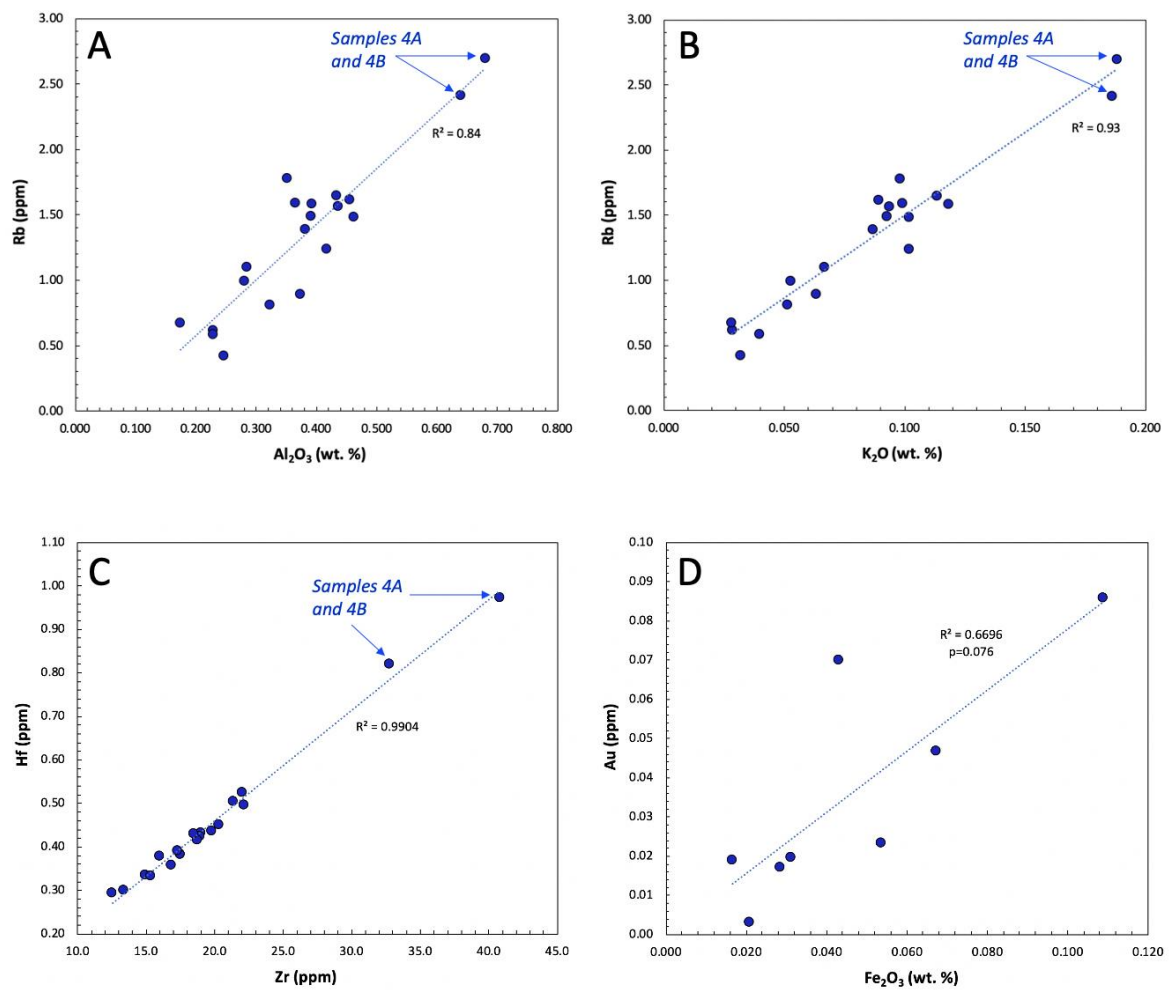
Figure 6. Geochemical trends observed in sampled Kinnikinic Quartzite. Samples 4A and 4B are consistently chemically anomalous compared to the remaining sample set. With respect to the compositional parameters shown above samples 4A and 4B are consistent enriched (panels A–C). For discussion see main text. (**A**) Al_2O_3 wt. % positively correlates with Rb (ppm), (**B**) K_2O wt. % positively correlates with Rb (ppm), (**C**) Zr (ppm) positively correlates with Hf (ppm), (**D**) weakly positive correlation between Fe_2O_3 (wt. %) and Au (ppm).
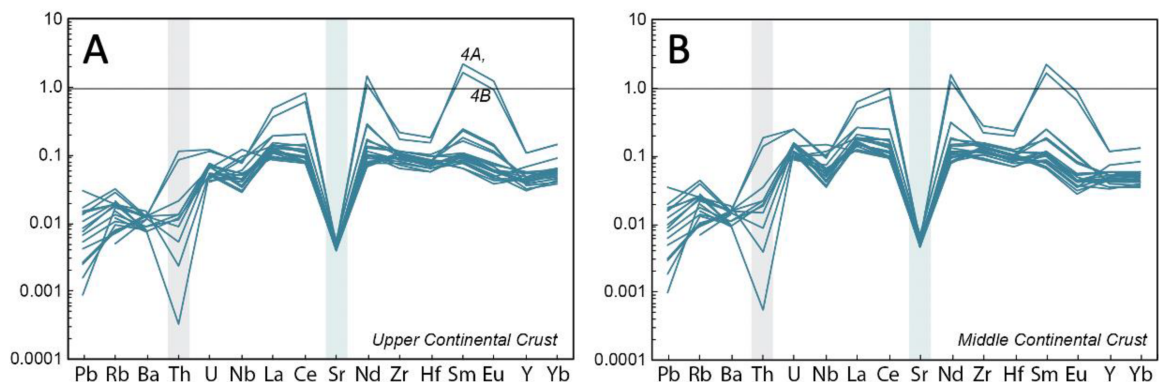
Figure 7. *Cont.*
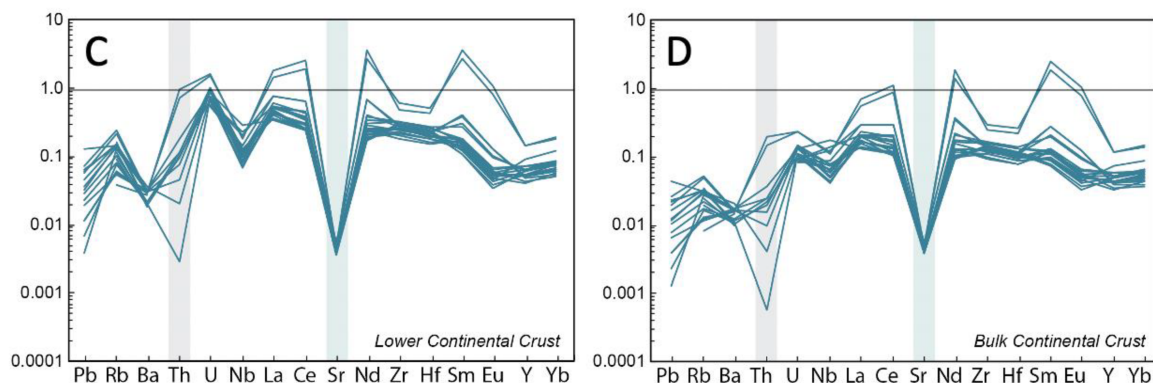
Figure 7. Normalization [37] of Kinnikinic Quartzite samples to Earth's bulk crustal reservoirs. (**A**) Upper Continental Crust, (**B**) Middle Continental Crust, (**C**) Lower Continental Crust, (**D**) Bulk Continental Crust.

4. Discussion

Quartzites in general are not widely established as ore materials, however there are some notable exceptions and contexts. Quartzites can serve primarily as ore bodies for gold, such as the extensive Witwatersrand Basin in South Africa [38,39] and the smaller gold paleo-placers of the Moeda Formation of Brazil [40]. Quartzite is also recognized as both an important historical building stone, such as the Bargiolina Quartzite from the western Alps, northern Italy [41]. The rock type is also a current and future building stone such as that observed in Benin, West Africa [42]. Quartzite also has desirable mechanical properties for use as an aggregate [43]. There are known occurrences of quartzite mining for producing silicon product, including investigations of nanostructured silicon from quartzite ore via hydrometallurgical processes combined with low energy wet blending, in a controlled atmosphere [44]. Quartzite is also extensively mined in Labrador, Canada for export to make silicon metal [45].

4.1. Mineralogy and Geochemistry Implications for Potential Future Mineral Resource Development

The sampled Kinnikinic quartzites of central Idaho are high silica (average wt. % SiO_2 of 99.11, n = 20). Specifically, the silica is associated with quartz grains and quartz cement, both of which contribute to the prominent Si peaks on all XRD patterns (Figure 2), and are well characterized via SEM-EDS (Figures 3 and 4). Minor to trace amounts of illite, potassium feldspar, and Fe-oxides are present as physically observed via SEM-EDS (Figure 3) and identified via bulk major element trends (see earlier). With respect to previous work on the Kinnikinic quartzite from the Arco Hills Silica and Gold Project, bulk wt. % SiO_2 contents reported in this study are consistent with values reported prior (97.32–99.48% SiO_2). Results presented here are, however, inconsistent with previous reports regarding the abundance of gold reported. Average gold concentrations, based on when detected, are 0.04 ppm (~0.001 oz./ton), and for all samples (60% were below detection) are 0.014 ppm (~0.0004 oz./metric ton). Commonly, gold concentrations at or above 5 ppm are sought for mine development [46]. However, some operations owing to scale and ore properties will support exploration at concentrations < 5 ppm, such as the Round Mountain operation in central Nevada with gold ore that commonly varies between 0.2 ppm and 1.2 ppm (Kinross USA Staff, Personal Communication 2015–2019). Even if gold concentrations were an order of magnitude higher in the Kinnikinic quartzite, it is highly unlikely that gold is economically recoverable given overall rock quality: low porosity and low permeability and the tentative association of gold with Fe_2O_3 content. Such ore properties are less than desirable, particularly for cyanide extraction methods [47].

Within the context of utilizing the Kinnikinic quartzite for the development of a plasma furnace operation in Butte County, Idaho, (for silicon metal), other byproducts potentially associated with waste streams are REEs. As gold has already been demonstrated as an economically challenging target within these contexts (see above and discussion later), the REEs are now considered. Chondrite-normalized REE

patterns for the sampled quartzite are summarized in Figure 8, alongside Earth's bulk crustal reservoirs. As shown, the quartzites are light-REE (LREE) enriched (La-Nd) and heavy-REE depleted (Dy-Lu).
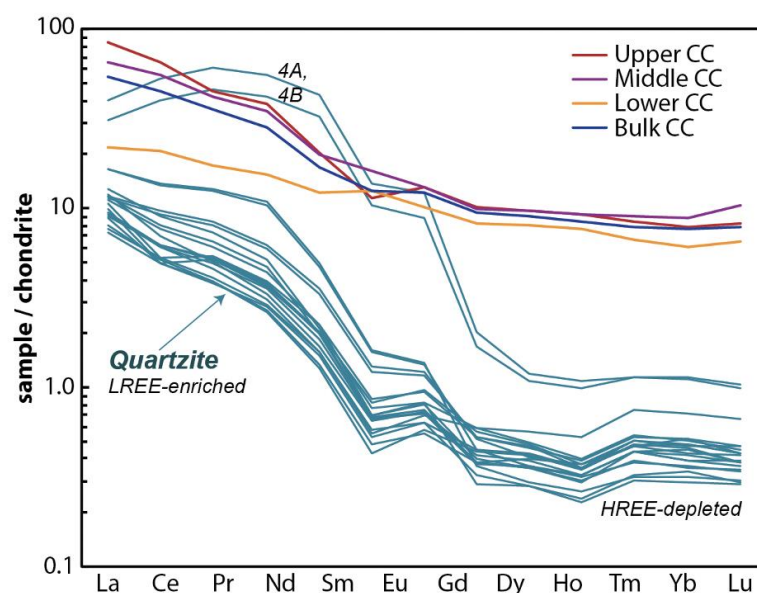
Figure 8. Normalization [37] of Kinnikinic Quartzite samples to chondrite. Normalizing values from Nakamura, 1974. For comparison, Earth's bulk geochemical reservoirs are also shown. Data from Rudnick and Gao (2003). As shown, the sampled Kinnikinic Quartzite is significantly depleted by 1–3 orders of magnitude in REEs compared to Earth's crustal values. See text for discussion.

Compared to Earth's bulk crustal reservoirs, they are consistently depleted by at least one order of magnitude. Again, however, there are exceptions associated with samples 4A and 4B, which display concave upward LREE patterns with clear Sm and Nd enrichments compared to crustal reservoirs and overall abundance enrichments compared to the sampled suite.

Rare earth element resources are a crucial component of the world's economy in both established and emerging markets, and in order to keep up with increasing consumer demand, new sources are going to need to be identified [6,7]. Establishing efficient approaches to recycling REEs is highly desired. Previous work has proposed that the extraction of REEs from mine-related waste could be one such approach [48]. None of the Kinnikinic quartzite samples considered in this study exhibit individual REE concentrations that could be considered economical. When considered within the context of a waste stream from plasma furnace methods, there is the potential for economically significant concentrations to be generated, however this would, of course, be significantly market dependent, and the pricing of REE is known to be volatile [16]. Ultimately, the economic viability of REE materials is likely to be tied to the viability of other resources (such as gold) in a given location. From the Kinnikinic quartzite, the total sum REE concentrations varied from 13 to 143 ppm, with an average concentration of 31 ppm and an associated standard deviation of 33 ppm. Samples 4A and 4B are enriched in total REEs relative to others. In the context of a hypothetical waste stream, assuming 100% removal of SiO_2, and 100% retention of average concentrations of total REEs, waste would have approximately 3400 ppm of total REEs. For sample material such as 4A and 4B, using a value of 143 ppm waste concentrations would be approximately 15,900 ppm. Th concentrations for these scenarios would be approximately 30 to 130 ppm and U concentrations would be approximately 13 to 35 ppm. The processes associated with extraction of REE from different host materials are, however, complex [49–51]. Certainly, the form and extractability of REEs in such a hypothetical waste stream would need to be comprehensively evaluated. Although REEs alone are likely not economically viable in such a process, the economics associated with potential gold may enable REEs to be a considered as a viable byproduct in the future.

It is noted here that more extensive mineralogical and geochemical exploration is needed to fully characterize and comprehend the nature of this potential resource. There are implications for plasma furnace utilization and basic economic constraints offered by the results, however, if the Kinnikinic quartzite were to be explored in the future, numerous other factors should also be considered. In particular, the quartzites' geotechnical properties, fuel costs, and health issues surrounding silica should be exposed to workers in order to prevent or mitigate against silicosis [52].

4.2. Implications for Plasma Furnace Utilization

Prior work has demonstrated that plasma furnace methods for producing silicon metal show promise for the development of large-scale production of solar cells [53–55]. Recycling of waste streams that are rich in REE, Au and other metals such as platinum group elements, indium, and gallium within these contexts may be a significant impetus for the broader implementation of recycling practices in the future. In the context of the sampled Kinnikinic quartzite from Butte County Idaho presented in this study, when present, gold concentrations in a hypothetical waste fraction (assuming 100% removal of SiO_2 with 100% retention of gold in the waste stream), would produce a waste product containing between 2 ppm (0.064 oz./metric ton) and 112 ppm (3.600 oz./metric ton) gold, with an average of 38 ppm of gold. For samples studied, our best-case scenarios yield that gold was detected in 40% of the samples, yielding an average gold concentration estimate of 15.2 ppm (0.488 oz/metric ton). Theoretically, this would be the waste stream yield as a result of plasma furnace processing. These are fully acknowledged as crude and optimistic estimates here, based only on the spot check sample set provided. The potential recovery of gold may be significantly much lower, owing to the fact that Fe and Cu would likely also be present in the waste stream. While crude, such gold concentrations would be of interest to mid and large size producers, and may be viable in the context of extracting gold alone, as ore material with greater than 5 ppm concentration is generally recognized as being viable [46].

The cause of the tentative correlation of gold and Fe_2O_3 contents in the Kinnikinic quartzite (Figure 6D) is unclear, but may be density related with gold being associated with Fe-oxides as inclusions or adsorption on Fe-oxides [56]. The presence of gold and Fe-oxide minerals are broadly recognized as having strong associations in a number of other contexts, including the well-characterized Olympic Dam deposit [57,58], in addition to laterite deposits [59]. The extraction of Au from Fe-oxide rich materials is, however, complex [47,60,61]. For future exploration purposes, a reasonable working hypothesis is that higher iron contents in the Kinnikinic quartzite will be associated with higher gold contents. Although highly speculative, and assuming a linear relationship based on the existing data for when gold is present (Figure 6D), a concentration of total iron (expressed here as Fe_2O_3) of approximately 8000 ppm would have an approximate concentration of 5 ppm gold. This has the potential to be an economic ore if certain challenges can be overcome during processing, such as the tight porosity. It is noted that Norris Lab's result of 0.398 oz./ton on select dark material (refer to Supplementary Materials) is consistent with the observations of the current study, where there is a positive correlation with iron with gold concentrations. Note that the Norris lab material was a concentrate and not bulk quartzite (see Supplementary Material).

The approach of this study could be applied to other known or potential resources. For example, China has used imported silica sand to produce polysilicon [62]. These sources could be further evaluated for potential plasma furnace processing. Moreover, of note is the St. Peter Sandstone across regions of Illinois and Missouri [63,64]. This is an ultra-mature quartz sandstone, which is poorly consolidated and may have more favorable properties for physical processing. Deposits of the St. Peter Sandstone are commonly mined for glass and proppant by minor controlled blasting, excavation and water techniques [65]. The Kinnikinic quartzite would likely require blasting, therefore creating significant dust and an associated possible risk of silicosis or lung disease for workers if not managed properly.

Not only are other geologic formations potentially more suitable for plasma furnace approaches (see above), but there are examples of mine waste recycling which may be more attractive, more

economically feasible, and have positive environmental impacts. Tailings and mine waste from quartzite ores can be a significant environmental problem and this is perhaps most evident in South Africa, with extensive impacts on the Witwatersrand reefs as a result of mining operations [66–70]. Limited recycling efforts have been explored within these contexts [71]. Detailed investigations of Witwatersrand tailings for recycling in the context of plasma furnace silicon metal production may be warranted, as there may be gold concentrations of interest. The ore is already granulated and it would be one approach to addressing the associated environmental health issues. Of concern, however, would be the associated uranium content [39].

Data from this investigation supports the position that reserve estimates, put forth by previous consulting reports, likely overestimated the potential gold resources of the Kinnikinic quartzite associated with the proposed site. However, the detailed mineralogical and geochemical work presented here suggests that further work is justified in the context of identifying the variation of (and source of) gold, REEs, and silica resources in the region. However, it appears unlikely that there are economic resources in the immediate vicinity. A broader, systematic mineralogical and geochemical survey of the Kinnikinic quartzite throughout East-Central Idaho and the region (Figure 1B) would generate a more statistically meaningful data set and work to identify potential regions of interest that could establish whether or not the Kinnikinic quartzite is of economic interest.

5. Conclusions

Gold concentrations in the sampled Kinnikinic quartzite of Central Idaho (maximum of 0.003 oz./ton) are inconsistent with those reported previously (0.012 to 0.031 oz./ton) from consulting reports. Silica content are, however, consistent at >96 wt. % SiO_2. Exploration for gold in this system should be considered economically high risk, based on the texture of potential ore and the potential association of iron with gold, making traditional cyanide heap leaching techniques potentially inviable. The observations of gold and REEs indicate, however, that broader, more regionally oriented work, could determine if there are statistically significant trends in elemental concentrations and associations. This would work to determine if better byproduct streams are possible and should be considered. The potential implementation of plasma furnace technology may open new resources for the green economy; however, detailed, integrated studies of targeted formations must be undertaken to understand the variability of potential byproduct composition. Results of this study suggest that detailed mineralogical and geochemical studies of other quartzites formations, the St. Peter Sandstone of Illinois and Missouri for example, are warranted within these contexts.

References

1. Wellmer, F.W.; Becker-Platen, J.D. Global Nonfuel Mineral Resources and Sustainability. *U.S.G.S. Circ.* **2016**, 1294. Available online: https://pubs.usgs.gov/circ/2007/1294/paper1.html (accessed on 21 May 2020).
2. McNish, S. 2018 Conversations that Matter: Precious Metals in the Green Economy. Vancouver Sun. Available online: https://vancouversun.com/news/local-news/conversations-that-matter-precious-metals-in-the-green-economy/ (accessed on 21 May 2020).
3. Straterra. The Minerals Industry is among Sectors of the NZ Society Where Great Strides Have Been Made of the Last 20 Years or so. 2018. Available online: https://www.straterra.co.nz/mining-in-nz/sustainability/green-minerals-and-the-green-economy/ (accessed on 20 May 2020).
4. Frost, H.S. Africa Can Lead Platinum-Fueled Hydrogen Economy. *Mining Weekly* **2019**. Available online: https://m.miningweekly.com/article/s-africa-can-lead-platinum-fuelled-hydrogen-economy-2019-09-20-1/rep_id:3861 (accessed on 21 May 2020).
5. UN Environment Programme 2020. How Minerals and Metals Companies Can Help Achieve 2030 Agenda for Sustainable Development. Available online: https://www.unenvironment.org/news-and-stories/story/how-minerals-and-metals-companies-can-help-achieve-2030-agenda-sustainable (accessed on 21 May 2020).
6. Chu, S. U.S. Department of Energy Critical Materials Strategy. 2011. Available online: https://energy.gov/sites/prod/files/DOE_CMS2011_FINAL_Full.pdf (accessed on 2 May 2020).
7. Golev, A.; Scott, M.; Erskine, P.D.; Ali, S.H.; Ballantyne, G.R. Rare earth supply chains: Current status, constraints and opportunities. *Resour. Policy* **2014**, *41*, 52–59. [CrossRef]
8. Armentrout, C.; Burke, M.; Silverstein, J.; Krekeler, M.P.S.; Nesbit, L.; Kidd, M.; Straub, K.; Newby, N.; Sellers, A. An unusual occurrence of silver in stream sediment from northern Breathitt County, Kentucky. *Southeast. Geol.* **2015**, *51*, 109–119.
9. McLeod, C.; Krekeler, M.P.S. Sources of extraterrestrial rare earth elements: To the Moon and beyond. *Resources* **2017**, *6*, 40. [CrossRef]
10. El-Kammer, A.; El-Wakil, M.; abd El-Rahman, Y.; Fathy, M.; Abdel-Azeem, M. Stream sediment geochemical survey of rare element in an arid region of the Hamadat area, central Eastern Desert, Egypt. *Ore Geol. Rev.* **2020**, *117*, 103287. [CrossRef]
11. Lemos, F.A.; Sobral, L.G.S.; Dutra, A.J.B. Copper electrowinning from gold plant waste streams. *Miner. Eng.* **2006**, *19*, 388–398. [CrossRef]
12. Geise, G.; LeGalley, E.; Krekeler, M.P.S. Mineralogical and geochemical investigations of silicate-rich mine waste from a Kyanite mine in Central Virginia: Implications for mine waste recycling. *Environ. Earth Sci.* **2011**, *62*, 185–196. [CrossRef]
13. Schellenbach, W.L.; Krekeler, M.P.S. Mineralogical and geochemical investigations of pyrite-rich mine waste from a Kyanite mine in Central Virginia with comments on recycling. *Environ. Earth Sci.* **2012**, *66*, 1295–1307. [CrossRef]
14. Schippers, A.; Hedrich, S.; Vasters, J.; Drobe, M.; Sand, W.; Willscher, S. Biomining: Metal recovery from ores with microorganisms. In *Geobiotechnology I. Advances in Biochemical Engineering/Biotechnology*; Schippers, A., Glombitza, F., Sand, W., Eds.; Springer: Berlin/Heidelberg, Germany, 2013; Volume 141, pp. 1–47.
15. Park, I.; Tabelin, C.B.; Jeon, S.; Li, X.L.; Seno, K.; Ito, M.; Hiroyoshi, N. A review of recent strategies for acid mine drainage prevention and mine tailings recycling. *Chemosphere* **2019**, *219*, 588–606. [CrossRef]
16. Fickling, D. Rare-Earth Prices Decline in China. *Wall Str. J.* **2011**. Available online: https://www.wsj.com/articles/SB10001424052702304760604576426501004377160 (accessed on 14 May 2020).
17. Taplin, N. Why Rare Earths Are a Low-Grade Weapon in Trade Fight. *Wall Str. J.* **2019**. Available online: https://www.wsj.com/articles/why-rare-earths-are-a-low-grade-weapon-in-trade-fight-11559821874 (accessed on 2 May 2020).
18. Yang, S. China Trade Fight Raises Specter of Rare-Earth Shortage. *Wall Str. J.* **2019**. Available online: https://www.wsj.com/articles/china-trade-fight-raises-specter-of-rare-earth-shortage-11559304000 (accessed on 4 May 2020).
19. Why the Gold Price Is Falling. Economist 2015. Available online: https://www.economist.com/the-economist-explains/2015/07/20/why-the-gold-price-is-falling (accessed on 2 May 2020).
20. Pierdzioch, C.; Risse, M.; Rohloff, S. A boosting approach to forecasting the volatility of gold-price fluctuations under flexible loss. *Resour. Policy.* **2016**, *47*, 95–107. [CrossRef]

21. The Mysterious Quiescence of the Gold Market. Economist 2017. Available online: https://www.econ omist.com/finance-and-economics/2017/04/12/the-mysterious-quiescence-of-the-gold-market (accessed on 4 May 2020).

22. Hobbs, S.W.; Hays, W.H.; Ross, R.J., Jr. The Kinnikinic quartzite of central Idaho—Redefinition and subdivision. *US Geol. Surv. Bull. 1254–J.* **1968**. [CrossRef]

23. James, W.C.; Oaks, R.Q. Petrology of the Kinnikinic quartzite (Middle Ordovician), East-central Idaho. *J. Sediment. Res.* **1977**, *47*, 1491–1511.

24. Baar, E.E. Determining the Regional-Scale Detrital Zircon Provenance of the Middle-Late Ordovician Kinnikinic (Eureka) Quartzite, East-Central Idaho, U.S. Master's Thesis, Washington State University, Pullman, WA, USA, 2009; p. 144. Available online: http://citeseerx.ist.psu.edu/viewdoc/download?doi=10.1. 1.427.3930&rep=rep1&type=pdf (accessed on 5 May 2020).

25. Map of Idaho Highlighting Butte County Available through the Public Domain. Available online: https: //en.wikipedia.org/wiki/Butte_County,_Idaho#/media/File:Map_of_Idaho_highlighting_Butte_County.svg (accessed on 14 May 2020).

26. Skipp, B.; Snider, L.G.; Janecke, S.U.; Kuntz, M.A. Geologic Map of the Arco 30 × 60 Minute Quadrangle, South-Central Idaho. Idaho Geological Survey. 2009. Available online: https://www.idahogeology.org/pro duct/gm-47 (accessed on 29 May 2020).

27. Gehrels, G.E.; Dickinson, W.R.; Ross, G.M.; Stewart, J.H.; Howell, D.G. Detrital zircon reference for Cambrian to Triassic miogeoclinal strata of western North America. *Geology* **1995**, *23*, 831–834. [CrossRef]

28. Malone, D.H.; Craddock, J.P.; McLaughlin, P.I.; Konstantinou, A.; McGillivray, K. Detrital zircon geochronology of the Bighorn Dolomite, Wyoming, USA: Evidence for Trans-Hudson dust deposition on the Western Laurentian carbonate platform. *J. Geol.* **2017**, *125*, 261–269. [CrossRef]

29. McGuire, J.D.; Malone, D.H.; Craddock, J.P.; Malone, S.J. Detrital zircon U-Pb geochronology of the Ordovician lander sandstone, Bighorn mountains, Wyoming. *Mt. Geol.* **2019**, *56*, 231–246. [CrossRef]

30. Gehrels, G.E.; and Dickinson, W.R. Detrital zircon provenance of Cambrian to Triassic Miogeoclinal and Eugeoclinal Strata in Nevada. *Am. J. Sci.* **1995**, *295*, 18–48. [CrossRef]

31. Gehrels, G.E. Introduction to detrital zircon studies of Paleozoic and Triassic strata in western Nevada and northern California. *Geol. Soc. Am. Spec. Pap.* **2000**, *347*, 1–17. [CrossRef]

32. Beranek, L.P.; Link, P.K.; Fanning, C.M. Detrital zircon record of mid-Paleozoic convergent margin activity in the northern U.S. Rocky Mountains: Implications for the Antler orogeny and early evolution of the North American Cordillera. *Lithosphere* **2016**, *8*, 533–550. [CrossRef]

33. Gehrels, G.; Pecha, M. Detrital zircon U-Pb geochronology and Hf isotope geochemistry of Paleozoic and Triassic passive margin strata of western North America. *Geosphere* **2014**, *10*, 49–65. [CrossRef]

34. Burke, M.; Rakovan, J.; Krekeler, M.P.S. A study by electron microscopy of gold and associated minerals from Round Mountain, Nevada. *Ore Geol. Rev.* **2017**, *91*, 708–717. [CrossRef]

35. Chen, P-Y. Table of Key Lines in X-ray Powder Diffraction Patterns of Minerals in Clays and Associated Rocks. *Indiana Dep. Nat. Resour. Geol. Surv. Occas. Pap.* **1977**. Available online: http://clay.uga.edu/courses/8 550/Chen_OP21.pdf (accessed on 21 May 2020).

36. Geochemical Earth Reference Model. Available online: https://earthref.org/KDD/ (accessed on 16 May 2020).

37. Rudnick, R.L.; Gao, S. Composition of the continental crust. *Treatise Geochem.* **2003**, *3*, 1–64.

38. Kirk, J.; Ruiz, J.; Chesley, J.; Titley, S.; Walshe, J. A detrital model for the origin of gold and sulfides in the Witwatersrand basin based on Re-Os isotopes. *Geochim. Cosmochim. Acta* **2001**, *65*, 2149–2159. [CrossRef]

39. Tucker, R.F.; Viljoen, R.P.; Viljoen, M.J. A review of the Witswatersrand Basin—The World's greatest goldfield. *Episodes* **2016**, *39*, 105–133. [CrossRef]

40. Minter, W.E.L.; Renger, F.E.; Siegers, A. Early Proterozoic gold placers of the Moeda Formation within the Gandarela Syncline, Minas Gerais, Brazil. *Econ. Geol. Bull. Soc. Econ. Geol.* **1990**, *85*, 943–951. [CrossRef]

41. Cavallo, A.; Dino, G.A. The Bargiolina, a striking historical stone from Monte Bracco (Piedmont, NW Italy) and a Possible Source of Industrial Minerals. *Sustainability* **2019**, *11*, 4293. [CrossRef]

42. Stein, K-J. Deposits of dimension stone in Benin and their classification after UNFCR. *Z. Dtsch. Gessllschaft Geowiss.* **2007**, *158*, 429–446. [CrossRef]

43. Cabello, M.L.; Peres, A.E.C.; Martins, A.H.; Pereira, C.A. Use of quartzite quarries wastes in civil construction. *Glob. Stone Congr.* **2013**, *548*, 135. [CrossRef]

44. Aliasgharzadeh-Polesangi, A.; Abdollah-Pour, H.; Farzin, Y.A. Nanostructured silicon production from quartzite ore by low-energy wet blending of the reagents, reduction in controlled atmosphere, and hydro metallurgy. *J. Mater. Res. Technol.* **2019**, *8*, 1014–1023. [CrossRef]

45. The Mineral Industry in Newfoundland and Labrador: Its Development and Economic Contributions. Government of Newfoundland and Labrador, Department of Natural Resources. *Geol. Surv.* **2020**. Available online: https://www.gov.nl.ca/nr/files/mines-geoscience-publications-openfiles-of-nfld2889.pdf (accessed on 21 May 2020).

46. Ridley, J. *Ore Deposit Geology*; Cambridge University Press: Cambridge, UK, 2013; p. 398.

47. Marsden, J.O.; House, C.I. *The Chemistry of Gold Extraction*; Society for Mining, Metallurgy and Exploration Inc.: Littleton, CO, USA, 2006; p. 682.

48. Goonan, T.G. Rare Earth Elements—End Use and Recyclability; Scientific Investigations Report. 2011–5094. *U. S. Geol. Surv.* **2011**. Available online: https://pubs.usgs.gov/sir/2011/5094/pdf/sir2011-5094.pdf (accessed on 2 May 2020).

49. Al-Thyabat, S.; Zhang, P. REE extraction from phosphoric acid, phosphoric acid sludge, and phosphogypsum. *Trans. Inst. Min. Metall. Sect. C-Miner. Process. Extr. Metall.* **2015**, *124*, 143–150. [CrossRef]

50. Huang, X.W.; Dong, J.S.; Wang, L.S.; Feng, Z.Y.; Xue, Q.N.; Meng, X.L. Selective recovery of rare earth elements form ion-adsorption rare earth element ores by stepwise extraction with HEH(EHP) and HDEHP. *Green Chem.* **2017**, *19*, 1345–1352. [CrossRef]

51. Maes, S.; Zhuang, W.Q.; Rabaey, K.; Alvarez-Cohen, L.; Hennebel, T. Concomittant leaching and electrochemcial extraction of rare earth elements from monazite. *Env. Sci. Tech.* **2017**, *51*, 1654–1661. [CrossRef]

52. NIOSH, N.D. Tips for Preventing Silicosis. Available online: https://arlweb.msha.gov/S&HINFO/SILICO/SILITIPS.pdf (accessed on 6 May 2020).

53. Miles, R.W.; Hynes, K.M.; Forbes, I. Photovoltaic solar cells: An overview of state-of-the-art cell development and environmental issues. *Prog. Cryst. Growth Charact. Mater.* **2005**, *51*, 1–42. [CrossRef]

54. Sörvik, A.I. Method for the Manufacture of Pure Silicon Metal and Amorphous Silica by Reduction OF Quartz (SiO2). World Intellectual Property Organization. Patent No. WO2007102745A1, 2007. Available online: https://patents.google.com/patent/WO2007102745A1/en (accessed on 21 May 2020).

55. Volokitin, O.; Vlasov, V.; Volokitin, G.; Skripnikova, N.; Shekhovtsov, V. Mathematical modeling of quartz particle melting process in plasma-chemical reactor. *AIP Conf. Proc.* **2016**, *1698*, 040013. [CrossRef]

56. Zhou, H.; Sun, X.; Cook, N.J.; Lin, H.; Fu, Y.; Zhong, R.; Brugger, J. Nano- to micron-scale particulate gold hosted by magnetite a product of gold scavenging by bismuth melts. *Econ. Geol.* **2017**, *112*, 993–1010. [CrossRef]

57. Reeve, J.S.; Cross, K.C.; Smith, R.N.; Oreskes, N. Olympic dam copper-uranium-gold-silver deposit. In *Geology and Mineral Deposits or Australia and Papau New Guinea*; Hughes, F.E., Ed.; Melbourne Australasian Institute of Mining and Metallurgy: Carlton, Australia, 1990; Volume 14, pp. 1009–1035.

58. Reynolds, L.J. Geology of the Olympic Dam Cu-U-Au-Ag-REE deposit. *MESA J.* **2001**, *23*, 4–11. Available online: http://www.geokniga.org/books/4804 (accessed on 21 May 2020).

59. Porto, C.G.; Hale, M. Mineralogy, morphology and chemistry of gold in the stone line lateritic profile of the Posse deposit, Central Brazil. *J. Geochem. Explor.* **1996**, *57*, 115–125. [CrossRef]

60. Al-Merey, R.; Hariri, Z.; Abu Hilal, I. Selective separation of gold from iron ore samples using ion exchange resin. *Microchem. J.* **2003**, *75*, 169–177. [CrossRef]

61. Bas, A.D.; Safizadeh Ghali, E.; Choi, Y. Leaching and electrochemical dissolution of gold in the presence of iron oxide minerals associated with roasted gold ore. *Hydrometallurgy* **2016**, *166*, 143–153. [CrossRef]

62. Dickinson, S. Rare Earth and Polysilicon. Does China Control Our Green Future? *China Bus.* **2010**. Available online: https://www.chinalawblog.com/2010/11/rare_earths_and_polysilicon_does_china_hold_our_green_future_in_its_hands.html (accessed on 6 May 2020).

63. Johnson, C.M.; Winter, B.L. Provenance analysis of lower Paleozoic cratonic quartz arenites of the North American midcontinent region U-Pb and Sm-Nd isotope geochemistry. *Geol. Soc. Am. Bull.* **1999**, *111*, 1723–1738. [CrossRef]

64. Konstantinou, A.; Wirth, K.; Craddock, J.P.; Malone, D.H.; Vervoort, J.D.; Davidson, C. Provenance of early Paleozoic quartz arenites, Midcontinent, USA. *J. Geol.* **2014**, *22*, 201–216. [CrossRef]

65. Davis, J.G. *St. Peter Sandstone Mineral Resource Evaluation. Proceeding of the 48th Annual Forum on the Geology of Industrial Minerals, Missouri, USA, 30 April–4 May 2012*; Conway, F.M., Ed.; Phoenix, Arizona, Arizona Geological Survey Special Paper: Scottsdale, AZ, USA, 2014; pp. 1–7. Available online: http://repository.azgs.az.gov/sites/default/files/dlio/files/nid1576/fgim-chap6-stpeterss_davis.pdf (accessed on 6 May 2020).

66. Naicker, K.; Cukrowska, E.; McCarthy, T.S. Acid mine drainage arising from gold mining activity in Johannesburg, South Africa and environs. *Environ. Pollut.* **2003**, *122*, 29–40. [CrossRef]

67. Winde, F.; Wade, P.; van der Walt, I.J. Gold Tailings as a Source of Waterborne Uranium Contamination of Streams—The Koekemoersruit. Klerksdopr Goldfield, South Africa as a Case Study—Part I of III: Uranium Migration Along the Aqueous Pathway. *Water SA* **2004**, *30*, 219–225. Available online: https://pdfs.semanticscholar.org/f41c/f7f6b9026fff84708b30e31a40f1ca7bf5f4.pdf (accessed on 6 May 2020).

68. Tutu, H.; McCarthy, T.S.; Cukrowska, E. The chemical characteristics of acid mine drainage with particulate reference to sources, distribution and remediation: The Witwatersrand Basin, South Africa as a case study. *Appl. Geochem.* **2008**, *23*, 3666–3684. [CrossRef]

69. Ojelede, M.E.; Annegarn, H.; Kneen, M.A. Evaluation of aeolian emissions from gold mine tailings on the Witswatersrand. *Aeolian Res.* **2012**, *3*, 477–486. [CrossRef]

70. Hansen, R.N. Inter-comparison geochemical modelling approaches and implications for environmental risk assessments: A Witswatersrand gold tailings source term characterization study. *Appl. Geochem.* **2018**, *95*, 71–84. [CrossRef]

71. Malatse, M.; Ndlovu, S. The Viability of Using the Witwatersrand Gold Mine Tailings for Brick Making. *J. South. Afr. Inst. Min. Metall.* **2015**, *115*, 321–326. Available online: http://www.scielo.org.za/scielo.php?script=sci_abstract&pid=S2225-62532015000400014 (accessed on 6 May 2020). [CrossRef]